Water Research, Volume 196, May 2021, Article number 117039
DOI: 10.1016/j.watres.2021.117039

An integrated approach using ozone nanobubble and cyclodextrin inclusion complexation to enhance the removal of micropollutants

Wei Fan [a], Wengang An [a], Mingxin Huo [a], Dan Xiao [b,*], Tao Lyu [c,*], Jingyu Cui [a].

[a] *School of Environment, Northeast Normal University, 2555 Jingyue Street, Changchun, 130117, China*

[b] *Jilin Academy of Agricultural Science, 1363 Shengtai Street, Changchun, 130033, China*

[c] *Cranfield Water Science Institute, Cranfield University, College Road, Cranfield, Bedfordshire, MK43 0AL, UK*

Corresponding authors: Dan Xiao, Email: xiaodan_nky@163.com

Tao Lyu, Email: T.lyu@cranfield.ac.uk

Abstract

Ozone (O_3) has been widely used for the elimination of recalcitrant micropollutants in aqueous environments, due to its strong oxidation ability. However, the utilization efficiency of O_3 is constrained by its low solubility and short half-life during the treatment process. Herein, an integrated approach, using nanobubble technology and micro-environmental chemistry within cyclodextrin inclusion cavities, was studied in order to enhance the reactivity of ozonisation. Compared with traditional macrobubble aeration with O_3 in water, nanobubble aeration achieved 1.7 times higher solubility of O_3, and increased the mass transfer coefficient 4.7 times. Moreover, the addition of hydroxypropyl-β-cyclodextrin (HPβCD) further increased the stability of O_3 through formation of an inclusion complex in its molecule-specific cavity. At a HPβCD:O_3 molar ratio of 10:1, the lifespan of O_3 reached 18 times longer than in a HPβCD-free O_3 solution. Such approach accelerated the removal efficiency of the model micropollutant, 4-chlorophenol by 6.9 times, compared with conventional macrobubble ozonation. Examination of the HPβCD inclusion complex by UV-visible spectroscopy and Nuclear Magnetic Resonance analyses revealed that both O_3 and 4-chlorophenol entered the HPβCD cavity, and Benesi-Hildebrand plots indicated a 1:1 stoichiometry of the host and guest compounds. Additionally, molecular docking simulations were conducted in order to confirm the formation of a ternary complex of HPβCD:4-chlorophenol:O_3 and to determine the optimal inclusion mode. With these results, our study highlights the viability of the proposed integrated approach to enhance the ozonation of organic micropollutants.

Keywords: advanced oxidation; chlorophenol; emerging organic contaminants; HPβCD; inclusion complex

1. Introduction

Organic micropollutants, such as pesticides (Lv et al., 2016), pharmaceutical and personal care products (Zhang et al., 2018), have been extensively detected in various aquatic systems, and pose a serious risk to the environment and to human health. A majority of such emerging contaminants have been reported to only achieve limited treatment efficiencies by conventional wastewater treatment plants, and thus development of alternative approaches toward more effective removal technologies is urgently required (Falås et al., 2018; Lyu et al., 2018). Due to a superior oxidation potential (2.07 V), the widely used ozone (O_3) treatment technology exhibits high capability for the oxidation of pharmaceuticals in drinking water (Prasse et al., 2012), remediation of antibiotics in wastewaters (Alexander et al., 2016), and removal of recalcitrant organic pollutants in groundwater (Hu and Xia, 2018). Molecular O_3 not only oxidises such pollutants directly, but also acts as a precursor to generate the hydroxyl radical (·OH) that is even more reactive as a nonselective oxidant (Kim et al., 2020). Nevertheless, efficient ozonisation is still restricted by low water solubility (e.g. < 10 mg L^{-1} in typical groundwater) and short half-life (typically < 1 h) (Khan and Carroll, 2020), and remains a significant technological challenge.

Many efforts have been made to enhance the ozonation process, including the addition of peroxides and thiosulfate (Yang et al., 2020), coupling ozonation with photocatalytic/electrolytic processes (Mehrjouei et al., 2015), and catalysis by metal ions or metal oxides (Nawrocki and Kasprzyk-Hordern et al., 2010). These approaches mainly focus on promoting the generation of ·OH from O_3, thus resulting in better oxidation of refractory organic contaminants (Yang et al., 2020). However, such optimisations still do not increase the solubilisation or prolong the reactivity of aqueous O_3.

Nanobubbles are defined as bubbles with a diameter of less than 1000 nm and possess special characteristics compared with normal macrobubbles, such as low buoyancy and long lifetimes (Zimmerman et al., 2011; Wang et al., 2020). In addition, the smaller bubbles have a greater surface area per unit volume and could therefore increase

the gas transfer rate into the surrounding water, significantly improving O_3 dissolution (Parmar and Majumder, 2015). Previous studies have demonstrated that the mixture of micro- and nanobubbles could increase the mass transfer coefficient (K_La) of O_3 by 2 times higher than that of macrobubbles (Gao et al., 2019). Moreover, it has been reported that nanobubbles can exist in water for days due to their low buoyancy (Ghaani et al. 2020). These unique characteristics of O_3 nanobubbles have been used to enhance the *in-situ* remediation of trichloroethylene-contaminated groundwater (Hu and Xia, 2018). Although the improvement of O_3 dissolubility and mass transfer rate through nanobubble technology could facilitate the ozonation process, the short half-life caused by the undesirable consumption of the oxidant, i.e. O_3 and ·OH, by non-target compounds and radical scavengers (Gardoni et al., 2012; Yuan et al., 2020) still limit the utilisation efficiency of O_3.

Currently, some chemical stabilisers have been developed to address this issue. Among them, addition of gentle organic acids such as acetic, propionic and short-chain fatty acids have been proven to increase the half-life of O_3 during ozone-based treatments (Alcantara-Garduno et al., 2008; Britton et al., 2020). Fan et al. (2020) reported that complete attenuation of O_3 could take 2.5 hours in 5% acetic acid solution (pH=2.56), which is 100 min longer than in pure water. Nevertheless, these acidic effluents would need further treatment before discharge, which would incur considerable hidden costs for the application. Another promising method was through use of cyclodextrins (CDs), which contain doughnut-shaped molecular structures with a hydrophilic outer shell and a hydrophobic inner cavity (Cai et al., 2015; Dettmer et al., 2017; Khan et al., 2018). This low polarity cavity can encapsulate dissolved size-matched guest compounds via coordination through various weak interactions (e.g. hydrophobic interactions, hydrogen bonds, and steric effects) and features molecular recognition capabilities(Fernández et al., 2019; Liu et al., 2020). Such inclusion complexes could increase the stabilisation of the enclosed molecules and prolong their lifespan, which would have the effect of also increasing the apparent solubility of low polarity organic compounds and thus their availability for removal (viz. sorption or degradation)

(Cheirsilp and Rakmai, 2016; Zhou et al., 2018; Zhou et al., 2020). According to this concept, Dettmer et al. (2017) initially investigated the hydroxypropyl-β-cyclodextrin (HPβCD):O_3 clathrate complex as an ozone stabilizer. The addition of HPβCD has been further proven to significantly enhance the ozonation of 1,4-Dioxane, Trichloroethylene and 1,1,1-Trichloroethane (Khan et al. 2019). Nevertheless, the molecular structures of the complexes and the dynamics of their formation need further study in order to reveal the underpinning mechanisms.

The purpose of this study was to investigate the combined approach of using O_3 nanobubbles and HPβCD to overcome the dual problems hitherto inherent in the ozonation process for remediation of organic pollutants. The reason for using HPβCD is that HPβCD is relatively inexpensive and well tolerated in humans (Gloud and Scott, 2005). The main hypothesis is that the O_3 nanobubbles could increase the solubility and transfer efficiency of O_3, then the dissolved ozone could enter into the cyclodextrin cavity which would inhibit their otherwise rapid decay. Therefore, in this study, the improvement of O_3 solubility and mass transfer rate, through application of nanobubble technology, was first examined. Furthermore, different HPβCD:O_3 molar ratios were utilised in order to investigate the lifespan of the complexed O_3, and the dynamics of decay of the generated reactive oxygen species (ROSs), i. e. ·OH and H_2O_2. The removal performance and degradation kinetics of 4-chlorophenol, a model micropollutant, were monitored in order to further evaluate the proposed integrated ozonation technique. In order to understand the mechanisms, UV-visible spectroscopy (UV-vis) and Nuclear Magnetic Resonance (NMR) analysis were used to characterise the HPβCD inclusion complex and molecular docking simulations were conducted to reveal probable modes of inclusion formation.

2. Materials and methods

2.1. Chemicals

Hydroxypropyl-β-cyclodextrin (HPβCD, $C_{63}H_{112}O_{42}$, 98%) was purchased from Yuanye Bio-Technology Co., Ltd (Shanghai, China). A typical organic micropollutant, 4-chlorophenol, was selected as the model contaminant in

this study, which exhibits high toxicity and persistence characteristics in an aquatic environment. Deionized (DI) water (>18.2 MΩ; Milli-Q Academic, Millipore, USA) was used to prepare all solutions.

2.2. Ozone nanobubble and macrobubble generation

Oxygen (99.5%, Juyang Co., Ltd, China) was used as the gas source for O_3 generation (CH-ZTW7G, Chuanghuan, China). The flow rate and concentration of the O_3 gas into a pressurized dissolution type nanobubble generator (Model XZCP-K-0.75, Xiazhichun, China) were approximately 0.5 L min^{-1} and 38 mg L^{-1}, respectively. The macrobubble aeration was prepared using a microporous plate diffuser (SB718, Songbao, China). The concentration and inflow rate of the O_3 for this diffuser were same as for nanobubble generation. The size and distribution of nanobubbles after generation were analysed with a Coulter Multisizer 4e (Beckman Coulter, Brea, USA). The size range of macrobubbles was estimated by analyzing a digital image acquired under strong light (3500 lumens, Magnaten D6, China), using ImageJ software (v 1.5, Schneider et al. 2012; Desai et al. 2019). The aqueous O_3 concentration was monitored using the indigo dye method (Wang et al. 2019). The volumetric mass transfer coefficient (K_La) of O_3 to water was determined during O_3 aeration according to the method reported by Fan et al. (2020), which can be calculated using equation as $K_La = \frac{ln\left(\frac{C_t}{C_s - C_t}\right)}{t}$, where C_t (mg L^{-1}) is the ozone concentration at the aeration time t and C_s (mg L^{-1}) is the saturated dissolved ozone concentration.

2.3. Ozone decay experiment

The decay kinetics of O_3 after the addition of HPβCD in O_3 nanobubble and macrobubble solutions were examined. Initially, water aliquots (50 mL) in amber glass bottles (100 mL volume) were aerated by O_3 nanobubble and macrobubble streams until O_3 concentrations reached 9 mg L^{-1} as mother liquor. In order to assess the impact of HPβCD on the O_3 half-life, the amount of the dissolved O_3 was then employed to calculate the addition of HPβCD, required to achieve molar ratios of HPβCD:O_3 of 0:1, 1:1, 3:1, 5:1 and 10:1. These bottles were then sampled by gastight syringe at various time intervals up to 72 hours, and both concentrations of aqueous O_3 and

generated ROSs, including ·OH and H_2O_2, were immediately analysed. Hydroxyl ·OH radicals were determined using a formaldehyde capturing method, while H_2O_2 was measured using the N, N-diethyl p-phenylenediamine/horseradish peroxidase method (Fan et al. 2020). The details for determining these free radicals were shown in the Supplementary Material (Text S1). All experiments were conducted in triplicate and terminated when the remaining O_3 concentration reached zero. Decay rates (k) of O_3 were calculated from the slopes of the $\ln(C_t/C_0)$-t regressive lines, where C_t denoted the O_3 concentration at time t, and C_0 was the initial O_3 concentration (6 mg L^{-1}). The half-life of O_3 was defined as the duration over which the initial O_3 concentration decreased by half. The lifespan of O_3 was defined as the time elapsed from the start of measurement until it could not be detected in the solution.

2.4. Integrated approach for 4-chlorophenol removal

The removal efficiencies of 4-chlorophenol during the ozonation process, under the integrated approach of O_3 nanobubble aeration and HPβCD addition, were evaluated. Water contaminated with 4-chlorophenol was prepared with an initial concentration of 30 mg L^{-1}. In the treatment groups, aeration with O3 macrobubbles or nanobubbles was applied to achieve initial O_3 concentrations of 6 mg L^{-1}. Meanwhile, HPβCD was added into the solution to achieve initial molar ratios of HPβCD: O_3 from 0:1 to 10:1 (section 2.3). A solution containing 4-chlorophenol at the same concentration, but without O_3 and HPβCD, were prepared as a control. The sampling procedure was the same as that described in section 2.3. The concentrations of 4-chlorophenol during treatment were determined by high-performance liquid chromatography (Agilent 1200 series, Agilent Technologies, Santa Clara, USA) with a C18 column (Text S1).

2.5. Characterisation of inclusion interactions and measurement of binding constants

Separate host (HPβCD) and guest (O_3 or 4-chlorophenol) stock solutions were mixed to create various molar ratios with or without nanobubbles, as described previously. The physiochemical properties of the guest molecule

caged within the host cavity were found to be very different from those of the free guest compounds (Karoyo and Wilson et al., 2019; Banjare et al. 2020). The host-guest complex formed from HPβCD:O_3 was monitored using UV-Visible spectrophotometry, and detection of the HPβCD:4-chlorophenol complex was conducted by a fluorescence titration method (Lin et al, 2020) and by NMR. The procedures for ^{1}H NMR and 2D ROESY NMR analyses are described in the Supplementary Material (Text S2). The binding constants of HPβCD-O_3 and HPβCD-4-chlorophenol inclusion complexes, indicative of inclusion potential, could be explained by the Benesi-Hildebrand equation (1) (Cai et al., 2015; Khan et al. 2019).

$$\frac{1}{\Delta F} = \frac{1}{\alpha K C_g [C_0]^n} + \frac{1}{\alpha C_g} \quad (1)$$

where ΔF is the change of absorbance of O_3 or fluorescence intensity of 4-chlorophenol in the presence or absence of HPβCD at different molar ratios of HPβCD: O_3; α is a constant related to the quantum yield of the complex and instrument itself; C_g is the concentration (mM) of the guest substrate (O_3 or 4-chlorophenol); C_0 is the concentration (mM) of HPβCD; n is the ratio of HPβCD to O_3 or 4-chlorophenol in the complex. K is the binding constant of the complex, corresponding to a ratio of the intercept to the slope.

2.6. Molecular docking simulation

The 3D structure of HPβCD was retrieved using PyMOL (The PyMOL Molecular Graphics System, Version 2.0 Schrödinger, LLC) from the native β-CD (PDB ID: 3CGT) in which the hydroxyl groups at the rim of the glucose unit were substituted with hydroxypropyl groups. Both the 3D structure of O_3 and 4-chlorophenol were structurally optimized with molecular mechanics method and plotted with Chem3D (v15.0, PerkinElmer Infomatics, Waltham, USA) (Zhang et al., 2017). To understand the interaction of HPβCD with a complexing ligand, molecular docking was executed using Autodock Tools (Version 4.2; Scripps Research Institute, San Diego, USA)) (Morris et al., 2009). The binding energies and molecular structures of the complexes were determined when O_3 and/or

4-chlorophenol were introduced into the HPβCD cavity. AutoDock's Lamarkian Genetic Algorithm (LGA) was applied to identify possible binding modes of O_3 and/or 4-chlorophenol with HPβCD through the entire process (Rasdi et al., 2019). A three-dimensional grid box of 52, 48, and 50 Å size in the x, y, and z directions was constructed using Autogrid (Scripps Research Institute, San Diego, USA) with a spacing of 0.375 Å centred on HPβCD. The grid box was appropriately designed to sufficiently enclose not only the HPβCD hollow region but also its exterior part. The interaction energy (ΔE) was then calculated by considering different molecular forces, including Van der Waals, electrostatics, hydrogen bonding, desolvation, and torsional (Rasdi et al., 2019). Different conformations with different binding energies were generated, and the most stable conformation with the lowest ΔE energy value was identified as the best binding mode in each docking simulation. The 3D model of the docking results was again visualized using PyMOL. The molecular structures of O_3, 4-chlorophenol, βCD, and HPβCD are illustrated in Fig. S1.

3. Results and Discussion

3.1. Enhanced solubilisation of O_3 by nanobubbles

The concentration of bubbles in the O_3 nanobubble aeration group achieved 2.16×10^5 particles mL^{-1}. Over 93.4% of the bubbles could be categorised as nanobubbles (<1000 nm) with a median diameter of 580 nm (Fig. 1a), whereas in the macrobubble aeration system, the average diameter of the bubbles was 1.82 mm, approximately 3.5 orders of magnitude higher (Fig. 1c). The O_3 concentration increased quickly after aeration began and then approached a quasi-steady state in both groups after 20 min (Fig. 1b). Bubble size distribution affects the O_3 content in water. If the mixed and pressured ozone remains in water as nanobubbles, they will have low buoyancies. Therefore, they rise slowly to the liquid surface or even shrink and collapse under liquid, consequently have longer residence time in the liquid and display certain stability (Parmar and Majumder, 2015). According to the classical two-film theory of gas absorption, the rate of mass transfer between two phases depends on the gas and liquid

phase mass-transfer coefficient, mass-transfer surface area to volume ratio, and the concentration gradient between the two phases, which can be described using Henry's law and Young-Laplace equation (Temesgen et al., 2017; Rabinowitz et al., 2020). The nanobubbles have high internal pressure (the Laplace pressure for a 100 nm bubble is about 14 atm) and a proportionally greater surface area. As the size of a nanobubble decreases the internal pressure rises, essentially pushing the internal ozone gas into the surrounding liquid. This synergetic effect thus can give an enhanced rate of gas transfer. Thus, the O_3 nanobubble aeration resulted in the oversaturation of O_3 with the dissolved O_3 concentration of 13.4 mg L^{-1} and mass transfer coefficient (K_La) of 0.179 min^{-1}, which were 1.7 times and 4.7 times higher than those (7.9 mg L^{-1} and 0.038 min^{-1}) measured from the macrobubble aeration group. Due to the smaller size of the nanobubbles, the increase of K_La was even 2 times higher compared with the value from the group utilising the mixture of micro- and nanobubble aeration (Gao et al., 2019).

Notably, a previous study has measured heterogeneous pressure inside nanobubbles by atomic force microscopy. This was further modelled by a molecular dynamics simulation and confirmed the high-gas-density state in nanobubbles (Zhang et al., 2006). The gas inside nanobubbles may exist as an aggregation, rather than an ideal gas phase, and the diffusion of the O_3 inside nanobubbles is likely to be slow and take place over a long period. Overall, the results demonstrated that O_3 nanobubble aeration could significantly increase solubilisation, and gas transfer efficiency, of O_3 and may sustainably supply O_3 to the surrounding water, which may enhance the ozonation of pollutants.

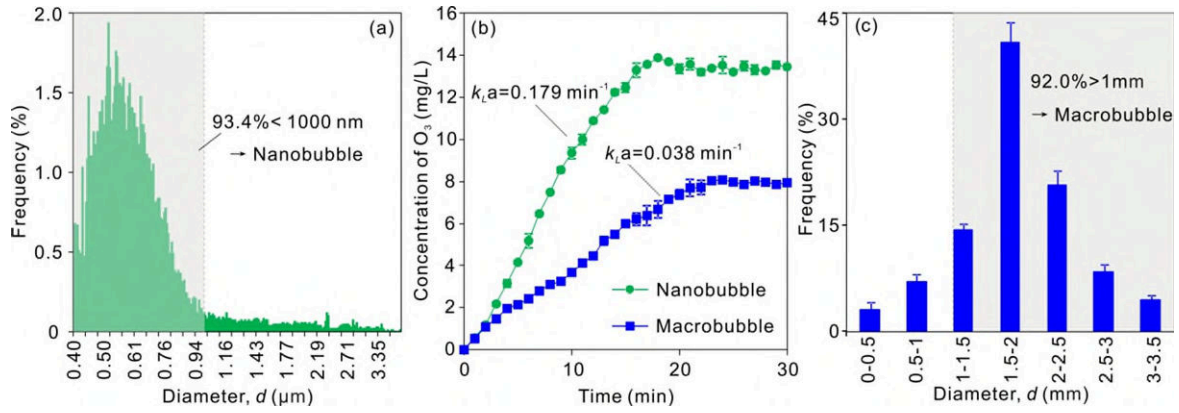

Fig. 1. (a) Size distribution of nanobubbles; (b) The time course of O_3 concentration during nanobubble and macrobubble aeration scenarios; (c) Size distribution of macrobubbles.

3.2. Improved stabilisation of O_3 by HPβCD inclusion complex

HPβCD is an environmentally-benign, glucose-based, non-toxic molecule containing hydroxypropyl groups attached on the outside of the macrocyclic cone (Fig. S1) (Bezamat et al. 2020). In order to conduct a comparative study to evaluate the effect of HPβCD on O_3 stabilisation, the decay of dissolved O_3 (Fig. 2a), from an initial O_3 concentration of 6 mg L^{-1}, and reactive oxygen species produced thereof, i.e. ·OH (Fig. 2b) and H_2O_2 (Fig. 2c), were monitored in both nanobubble and macrobubble aeration groups.

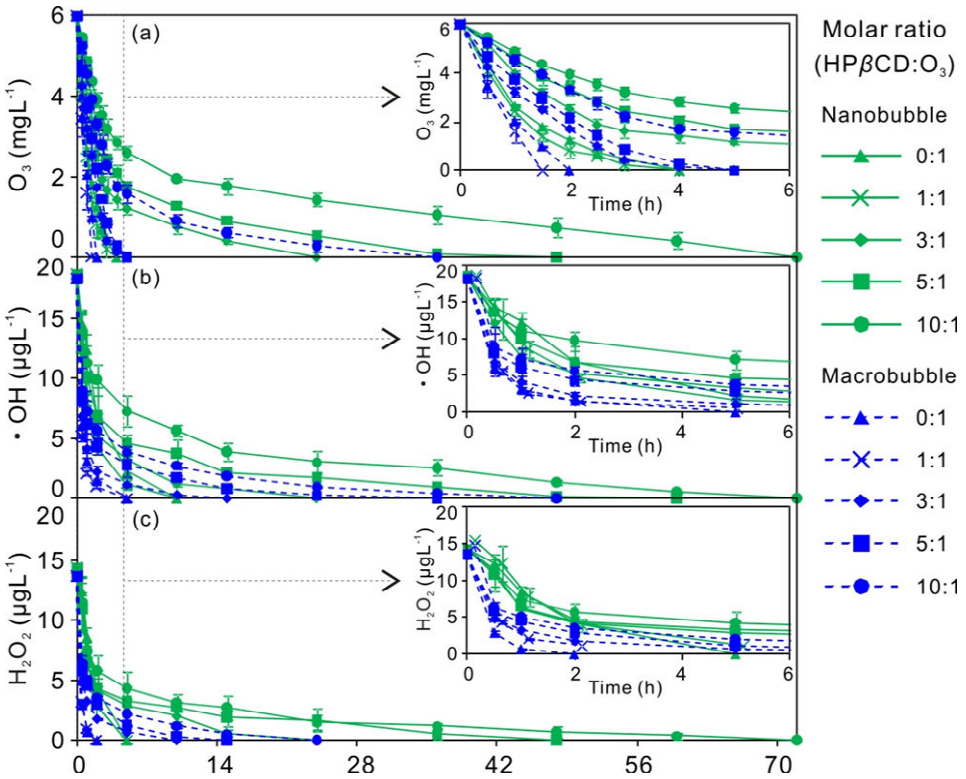

Fig. 2. Ozone decay (a), and produced reactive oxygen species, ·OH (b) and H_2O_2 (c), after nanobubble and macrobubble aeration under different HPβCD:O_3 molar ratios.

In HPβCD-free water (HPβCD:O_3 molar ratio of 0:1), aerated by macrobubbles, the lifespan of O_3 was approximately 1.75 h with a decay rate (k) of 1.15 h^{-1} (Fig. 2a and Table 1). As the hydroxypropyl group of HPβCD

could be oxidised, the ring in glycosides remains stable in the presence of oxidants, including O_3 (Manhas et al., 2007; Dettmer et al., 2017). Addition of small amounts of HPβCD, e.g. HPβCD:O_3 molar ratio below 1:1, could not slow down the decay of O_3 (Fig. S2). In the current study, along with the increase of HPβCD:O_3 molar ratio from 1:1 to 10:1 in the macrobubble aerated group, the O_3 decay rates decreased from 1.27 to 0.29 h^{-1} with a prolonged lifespan of up to 30 h (Fig. 2a and Table 1). This observation was mainly attributed to the molecular dimensions of the β-CD cavity which could readily form inclusion complexes through host-guest interactions (Szente et al., 2018). Khan et al. (2019) reported that significant amounts of O_3 and/or contaminants could enter the clathrate cavity and thus enhance their interaction through proximity effects. More importantly, the O_3 decay rates (0.19-0.95 h^{-1}) in the O_3 nanobubble aeration group were 0.49-0.75 times lower, and O_3 lifespans (3.5-66 h) were 2.00-9.33 times higher, than those determined from the macrobubble aeration group, at the same HPβCD:O_3 molar ratio (Fig. 2a and Table 1). The aforementioned higher mass transfer efficiency and longevity of nanoscale O_3 bubbles may have further contributed to the stabilization of O_3, displaying a synergistic effect with HPβCD.

Table 1 The lifespan and decay rates of O_3 in nanobubble and macrobubble aeration groups under different HPβCD:O_3 molar ratios

HPβCD:O_3	O_3 lifespan (h)		O_3 decay rates (h^{-1})	
molar ratio	macrobubble	nanobubble	macrobubble	nanobubble
0:1	1.75	3.50	1.15	0.83
1:1	1.25	3.50	1.27	0.95
3:1	4.50	19.50	0.66	0.43
5:1	4.50	42.00	0.57	0.28
10:1	30.00	66.00	0.29	0.19

In addition, the ROSs produced upon the decomposition of O_3 play a crucial role for removal of pollutants through ozonation (Kim et al., 2020). Thus, nanobubble-HPβCD-mediated O_3 decay kinetics in different scenarios were further confirmed by the detection of ·OH and H_2O_2 (Fig. 2b and 2c). The ·OH and H_2O_2 could be detected in macrobubble aeration groups in the initial 2-30 h (Fig. 2 and Table 1), while they remained from 0.16-1.32 and 0.37-0.66 μg L^{-1} after 36 h in the nanobubble aeration groups, under various HPβCD:O_3 molar ratios. The results confirmed that the addition of HPβCD could extend the lifetime of O_3 and promote the production of ROSs. Moreover, these functions were strengthened under the application of O_3 nanobubbles.

3.3. The integrated approach for 4-chlorophenol removal

The decomposition of 4-chlorophenol was investigated and comparisons made between the nanobubble and macrobubble ozonation processes at different HPβCD:O_3 molar ratios (Fig. 3). In the absence of HPβCD, the removal efficiency of 4-chlorophenol was significantly higher in nanobubble aeration group (28.33%) compare with that (11.51%) in the macrobubble aeration group, while the removal rate was less than 2% in the blank control tests (0:0 in the nanobubble ozonation group, Fig. 3). Another blank control test was also conducted by mixing 4-chlorophenol and HPβCD without ozonation, and the concentration of 4-chlorophenol showed very slight change (< 3%) in this case. Removal of 4-chlorophenol was enhanced with increasing HPβCD addition, until at a HPβCD:O_3 molar ratio of 10:1, removal of up to 79.0% and 51.0% in the nanobubble and macrobubble aeration groups, respectively, were observed. At each HPβCD:O_3 molar ratio, the application of O_3 nanobubbles always resulted in 12.1-146.15% higher removal efficiencies of 4-chlorophenol compared with treatment with macrobubbles. The removal efficiency at HPβCD:O_3 molar ratio of 10:1 by nanobubble ozonation was up to 6.9 times higher when compared with the 'normal' O_3 macrobubble treatment without addition of HPβCD.

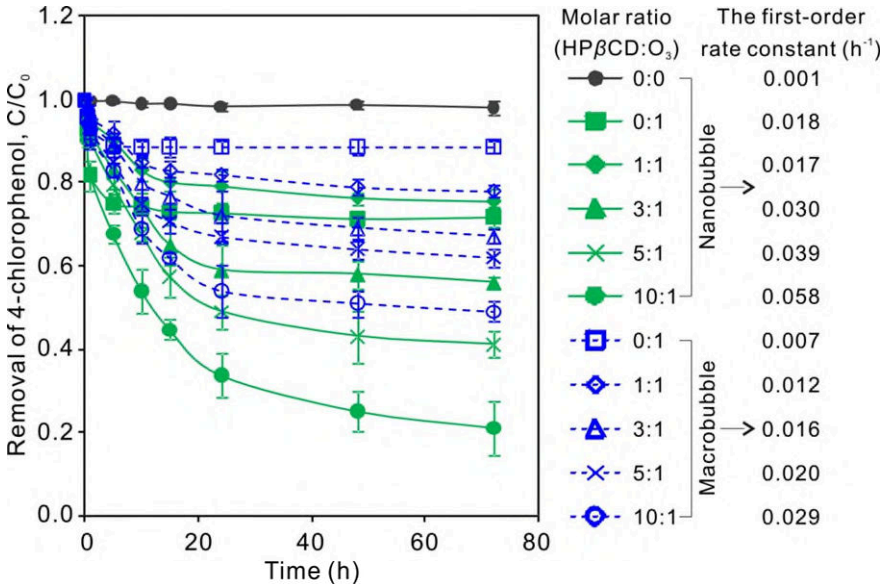

Fig. 3. Removal of 4- chlorophenol by nanobubble and macrobubble ozonation processes at different HPβCD: O_3 molar ratios (0:1 to 10:1).

Benitez et al. (2000) reported that the ozonation process of 4-chlorophenol could be described by a first-order kinetics model, which was also applied to the current study. First-order rate constants, estimated from the removal dynamics of 4-chlorophenol (Fig. 3) in the nanobubble emulsion, were 0.017, 0.030, 0.039, and 0.058 h^{-1} for HPβCD:O_3 molar ratios of 1:1, 3:1, 5:1, and 10:1, respectively. In contrast, the constants were 0.012, 0.016, 0.020, and 0.029 h^{-1} from the corresponding macrobubble ozonation process. Both O_3 and ROSs could contribute to the oxidisation of organic micropollutants (Van Aken et al. 2019), thus, the prolonged survival of O_3 and ROSs (Fig. S3) led to enhanced removal efficiency of 4-chlorophenol from the integrated approach of nanobubbles and addition of HPβCD (Fig. 3).

3.4. Measurement of inclusion complex binding

Binding constants were evaluated by analysing the variation of the absorbance of O_3 and the fluorescence emission intensity of 4-chlorophenol with host (HPβCD) concentration . O_3 has a characteristic absorption peak at 260 nm, which is clearly different from the adsorption spectrum of HPβCD (Fig. S4). Moreover, the excitation wavelength maximum of 4-chlorophenol was noted around 330 nm, where the fluorescent response of HPβCD was

very weak (Fig. S5). Notably, the absorbance of O_3 decreased with increasing concentration of HPβCD, while the fluorescence intensity of 4-chlorophenol increased. These two aspects are consistent with previous studies on the formation of inclusion compounds with HPβCD (Khan et al. 2019; Faisal et al., 2020). The response of absorbance of O_3 was attributed to the high electron density in the cavity of HPβCD, which could cause alteration in the valence electron characteristics in the O_3 molecule, an increase in the difference in electron transition energy and a decline in the electron transition probability (Shi and Zhou, 2011). The increase in rigid planarity, caused by the insertion of 4-chlorophenol into the hydrophobic cavity of HPβCD (Lin et al, 2020) may be responsible for the increase in intensity of fluorescence of 4-chlorophenol.

The Benesi-Hildebrand plots indicated that 1/[HPβCD] values displayed a positive linear relationship with the $1/\Delta F$ values of both O_3 and 4-chlorophenol (Fig. 4), suggesting that the stoichiometry of host and guest complexes was 1:1 in this study (n=1). The average inclusion constant K for O_3 and 4-chlorophenol with microbubble treatment were 0.75 mM^{-1} and 17.56 mM^{-1}, respectively, whereas they were determined to be 1.50 mM^{-1} and 18.06 mM^{-1} with nanobubbles, respectively. Although the presence of nanobubbles showed a negligible impact on the K of the HPβCD-4-chlorophenol complex, however, it significantly increased the K of the HPβCD-O_3 complex. It may be observed that the regression line of of data from the nanobubble aerated group yields larger intercept and smaller slope values than that of data measured from the macrobubble aeration group (Fig. 4a, Fig. S6). It has been reported that the host-guest interaction can be judged by calculation of the Gibbs energy of binding ΔG, $\Delta G=-RT\ln K$ (Srinivasana et al, 2012), where, R=8.314 J mol^{-1} K^{-1} (the gas constant per molecule), and K is the Kelvin temperature (294.3 K). The calculated ΔG herein were -16.20 and 17.89 kJ mol^{-1} for the HPβCD-O_3-macrobubble and HPβCD-O_3-nanobubble systems, while they were -23.91 and -23.98 kJ mol^{-1} for HPβCD-macrobubble-4-chlorophenol and HPβCD-nanobubble-4-chlorophenol complexes, respectively. Since the values of ΔG were all negative, the inclusion process proceeded spontaneously at the test temperature and the

complex formation was demonstrated as an exergonic process (Khan et al. 2019).

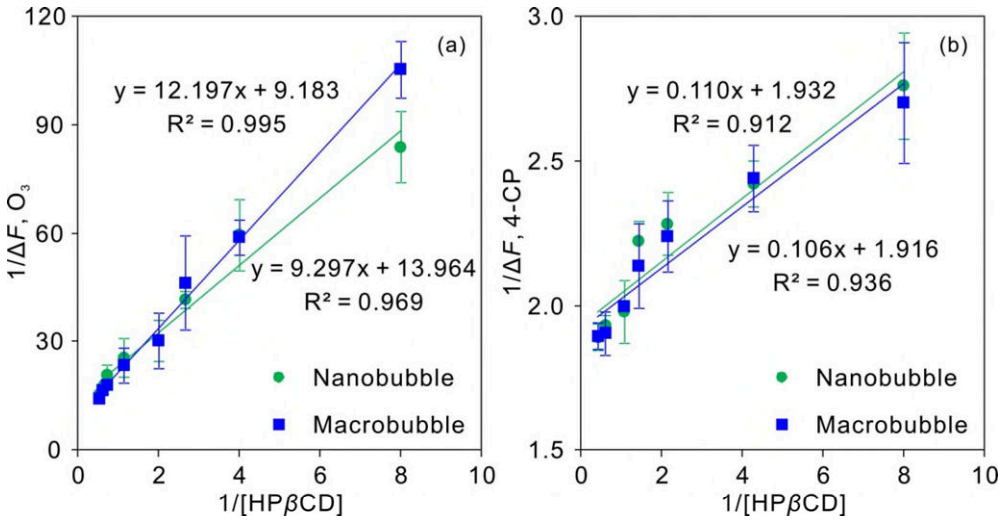

Fig. 4. Benesi-Hildebrand plots for O_3 and 4-CP in macrobubble and nanobubble aerated solutions at different HPβCD:O_3 molar ratios (0.5:1 to 15:1). The lines represent regression results used for binding equilibrium analyses.

3.5. Characterisation of inclusion complexes

The HP*β*CD:O_3 inclusion complex can be effectively detected using spectrophotometry. The optimum adsorption wavelength of O_3 was 260 nm, while HP*β*CD recorded no absorbance at this wavelength. The absorbance of O_3 increased upon the addition of HP*β*CD at a specific time (Fig. 5), and the absorbance for specific HP*β*CD:O_3 scenarios decreased gradually over time. A slight bathochromic shift (2~3 nm) was observed with increasing concentrations of HP*β*CD (Fig. S7), which has been reported previously with other guest molecules and has been explained in terms of a change in the environment of the molecule as it is included within the CD cavity (Hendy and Breslin, 2011; Lin et al, 2020). Usually, O_3 would have been completely degraded after 1-3 hour in DI water (Dettmer et al., 2017), however in this study, absorption peaks were still observed even after 12 h in the presence of HP*β*CD (Fig 5a and Fig. S7). These variation of absorbance intensity with time suggested that the formation of the inclusion complex is reversible. Thus HP*β*CD acted as “sustained-release capsules” for ozone

oxidation.

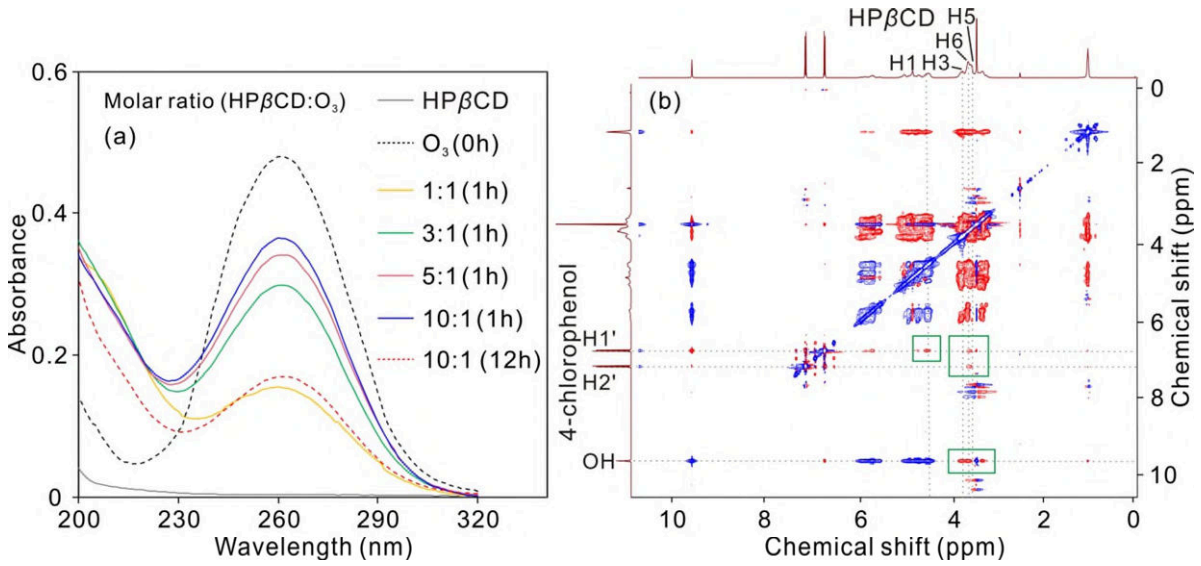

Fig. 5. (a) UV spectra of O_3 in the absence and presence of HPβCD at varying molar ratios of HPβCD: O_3. (b) 2D ROSEY spectra of HPβCD complexes with 4-CP.

The formation of an inclusion complex can affect the protons of the HPβCD and 4-chlorophenol molecules, which then results in changes in their chemical shifts (δ) in ^{1}H NMR spectra (Fig. S8) (Hendy and Breslin, 2011). Once a 4-chlorophenol molecule is placed inside the HPβCD cavity, the internal protons of HPβCD are involved in upfield shift changes of Δδ (for H3, Δδ=0.021; for H5, Δδ=0.015). For 4-chlorophenol, a shift of H1' (0.001), H2' (-0.008), and -OH (0.004) were synchronously observed. This internal interaction for HPβCD:4-chlorophenol was further elucidated by 2D ROESY NMR (Fig. 5b). Cross peaks in the two-dimensional plot indicate the intermolecular Nuclear Overhauser Effects (NOEs) between the 4-chlorophenol and HPβCD cavity protons. Of note, a strong cross-peak indicated interaction between proton H3 of HPβCD (δ= 3.764) and the hydroxyl group of the proton from 4-chlorophenol (δ= 9.657). These cross-peaks are marked by green boxes in Fig. 5b. The close proximity of these protons (distance less than 4 Å) indicated the inclusion of 4-chlorophenol into the HPβCD cavity (Adhikari et al., 2018).

3.6. Molecular docking simulation of inclusion complexes

To further elucidate the inclusion geometry of O_3 and 4-chlorophenol with HPβCD, molecular docking simulations were carried out, which can indicate how O_3 and 4-chlorophenol molecules could be arranged inside the HPβCD cavity in energetically favourable orientations (Gupta, et al., 2018; Rasdi et al., 2019). Five conformations with different binding energies for each scenario were generated, and their docking configurations and interaction energies are shown in Tables S1- S3. The high absolute value of the binding energy means high affinity between host and guest, and thus a more stable inclusion complex (Cai et al., 2015; Khan et al. 2019). Fig. 6 shows the most stable structure based on the docking simulations. The lowest binding energy was -2.12 kcal mol^{-1} for the stable docking conformation of HPβCD: O_3. HPβCD cavity is non-polar and hydrophobic, while O_3 is hydrophobic with very low polarity. This triggers a weak attractive force to trap O_3 inside the HPβCD cavity.

For the complex of HPβCD:4-chlorophenol, two different binding orientations with the same lowest binding energy -4.20 kcal mol^{-1} were calculated. The docking results suggested that 4-chlorophenol can insert, slantwise, into the cavity of HPβCD (Fig. 6b and c). The -OH group of 4-chlorophenol is always contained inside the cavity in either inclusion mode, which substantiated the results of 2D NMR analysis (Fig. 5b). We speculated that the -OH group in 4-chlorophenol is able to undertake hydrogen bonding with -OH groups inside the HPβCD cavity. Due to the free rotation of the hydroxypropyl on the narrower rim which would lead to a steric effect, the most likely mode of complexation would be an insertion into the cavity from the wider rim (Ge et al., 2011). Note that the -Cl group in 4-chlorophenol locates near the narrower rim in both docking configurations (Fig. 6b and c), 4-chlorophenol may enter the cavity with the relatively hydrophobic group -Cl leading. This is verified by the upfield shifts in the ^{1}H NMR signals for H3, compared to H5 (Fig. 5b). The docking results illustrated in Fig. 6d indicated the formation of ternary structures where 4-chlorophenol and O_3 form inclusion complexes within the HPβCD cavity. The optimal binding energy was -3.00 kcal/mol for HPβCD:4-chlorophenol:O_3 complex. Therefore, both 4-chlorophenol and O_3 are thermodynamically favoured to partition into HPβCD, which would increase their

relative concentrations and place them closer in order to facilitate reaction with each another. These results confirm that increased reactivity within the cavity leads to the observed enhanced oxidation performance.

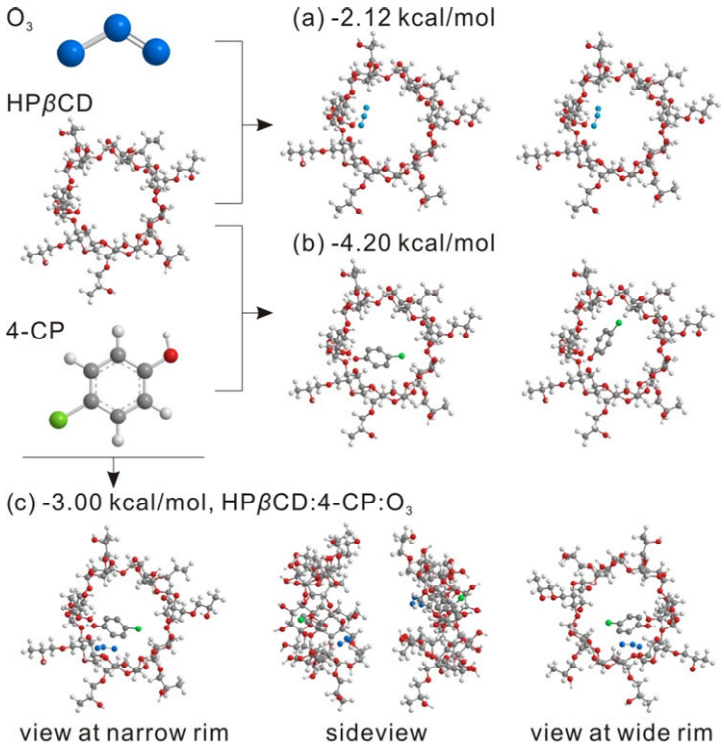

Fig. 6. Complexed structures of HPβCD:O_3 (a), HPβCD:4-chlorophenol (b), two binding orientations with the same interaction energy were presented herein; and HPβCD:4-chlorophenol:O_3 (c) with optimal interaction energy from molecular docking. In this figure, 4-chlorophenol is denoted by 4-CP.

4. Conclusions

This study developed a promising approach by coupling nanobubble technology and the addition of HPβCD in order to enhance the ozonation of an organic micropollutant in artificial contaminated water. Nanobubbles were found to promote the solubilisation and mass transfer of O_3, and also benefitted from the formation of inclusion complexes in the cavities of HPβCD, compared with conventional macrobubbles. The presence of HPβCD contributed to the stabilisation of O_3 by inclusion complexation, thereby extending the lifespan of O_3 from about one hour to dozens of hours. By addressing the two common drawbacks of ozonation, solubilisation and bubble longevity, the maximum removal efficiency of the target micropollutant, 4-chlorophenol, was 6.9 times higher,

when compared with the 'normal' O_3 macrobubble treatment. Investigation into possible mechanistic processes revealed that significant amounts of O_3 and/or 4-chlorophenol could enter the HPβCD cavity through various means. Molecular modelling confirmed the formation of ternary complexes of HPβCD:4-chlorophenol:O_3 and visual configurations of possible inclusion modes were generated. Overall, nanobubbles worked as an "O_3 bank" to supply O_3 and that HPβCD facilitated the entrapment of both the contaminant target and O_3 in close proximity. This intimate co-location of reactants and enhancement of reactivity within the HPβCD cavity resulted in increased 4-chlorophenol oxidation.

Acknowledgements

This work was funded by the National Natural Science Foundation of China (NSFC No. 51978135, 51908062, and 51678121). It was also supported by the Scientific and Technological Development Plan Project of Jilin Province (No. 20200201042JC) and the Fundamental Research Funds for the Central Universities, China (2412019ZD004).

References

Adhikari, S., Daftardar, S., Fratev, F., Rivera, M., Sirimulla, S., Alexander, K., Boddu, S.H.S., 2018. Elucidation of the orientation of selected drugs with 2-hydroxylpropyl-β-cyclodextrin using 2D-NMR spectroscopy and molecular modeling. Int. J. Pharm. 545, 357-365.

Alcantara-Garduno, M.E., Okuda, T., Tsai, T.Y., Nishijima, W., Okada, M., 2008, Experimental and mathematical evaluation of trichloroethylene removal from saturated soil using acetic acid with saturated ozone, Sep. Purif. Technol. 60, 299-307.

Alexander, J., Knopp, G., Dotsch, A., Wieland, A., Schwartz, T., 2016. Ozone treatment of conditioned wastewater selects antibiotic resistance genes, opportunistic bacteria, and induce strong population shifts. Sci. Total. Environ. 559, 103-112.

Banjare, M.K., Behera, K., Banjare, R.K., Pandey, S., Ghosh, K.K., 2020. Inclusion complexation of imidazolium-based ionic liquid and β- cyclodextrin: A detailed spectroscopic investigation. J. Mol. Liq. 302, 112530.

Benitez, F.J., Beltran-Heredia, J., Acero, J.L., Rubio, F.J., 2000. Rate constants for the reactions of ozone with chlorophenols in aqueous solutions. J. Hazard. Mater. 79, 271-285.

Bezamat, J.M., Yokaichiya, F., Dias Franco, M.K.K., Castro, S.R., de Paula, E., Cabeça, L.F., 2020. Complexation of the local anesthetic pramoxine with hydroxypropyl-beta-cyclodextrin can improve its bioavailability. J. Drug. Deliv. Sci. Technol. 55, 101475.

Britton, H.C., Draper, M., Talmadge, J.E., 2020. Antimicrobial efficacy of aqueous ozone in combination with short chain fatty acid buffers. Infect. Prev. Pract. 2, 100032.

Cai, X., Liu, Q., Xia, C., Shan, D., Du, J., Chen, J., 2015. Recyclable capture and destruction of aqueous micropollutants using the molecule-specific cavity of cyclodextrin polymer coupled with KMnO4 oxidation. Environ. Sci. Technol. 49, 9264-9272.

Cheirsilp, B., Rakmai, J., 2016. Inclusion complex formation of cyclodextrin with its guest and their applications. Biol. Eng. Med. 2, 1-6.

Desai, P.D., Ng, W.C., Hines, M.J., Riaz, Y., Tesar, V., Zimmerman, W.B., 2019. Comparison of bubble size distributions inferred from acoustic, optical visualisation, and laser diffraction. Colloids and Interfaces. 3, 65.

Dettmer, A., Ball, R., Boving, T.B., Khan, N.A., Schaub, T., Sudasinghe, N., Fernandez, C.A., Carroll, K.C., 2017. Stabilization and prolonged reactivity of aqueous-phase ozone with cyclodextrin. J. Contam.Hydrol. 196, 1-9.

Faisal, Z., Fliszár-Nyúl, E., Dellafiora, L., Galaverna, G., Dall'Asta, C., Lemli, B., Kunsági-Máté, S., Szente, L., Poór, M., 2020. Interaction of zearalenone-14-sulfatewith cyclodextrins and the removal of the modified mycotoxin from aqueous solution by beta-cyclodextrin bead polymer. J. Mol. Liq. 310, 113236.

Falås, P., Wick, A., Castronovo, S., Habermacher, J., Ternes, T.A., Joss, A., 2016. Tracing the limits of organic micropollutant removal in biological wastewater treatment. Water Res. 95, 240-249.

Fan, W., An, W., Huo, M., Yang, W., Zhu, S., Lin, S., 2020. Solubilization and stabilization for prolonged reactivity of ozone using micro-nano bubbles and ozone-saturated solvent: A promising enhancement for ozonation. Sep. Purif.Technol. 238, 116484.

Fernández, M.A., Silva, O.F., Vico, R.V., Rossi, R.H., 2019. Complex systems that incorporate cyclodextrins to get materials for some specific applications. Carbohydr.Res. 480, 12-34.

Gao, Y., Duan, Y., Fan, W., Guo, T., Huo, M., Yang, W., Zhu, S., An, W., 2019. Intensifying ozonation treatment of municipal secondary effluent using a combination of microbubbles and ultraviolet irradiation. Environ.Sci. Pollut. Res. 26, 21915-21924.

Gardoni, D., Vailati, A., Canziani, R., 2012. Decay of ozone in water: a review. Ozone Sci. Eng. 34, 233-242.

Ge, X., He, J., Qi, F., Yang, Y., Huang, Z., Lu, R., Huang, L., 2011. Inclusion complexation of chloropropham with -cyclodextrin: Preparation, characterization and molecular modeling. Spectrochim. Acta A Mol. Biomol. Spectrosc. 81, 397-403.

Ghaani, M.R., Kusalik, P.G., English, N.J., 2020. Massive generation of metastable bulk nanobubbles in water by external electric fields. Sci. Adv. 6, eaaz0094.

Gould, S., Scott, R.C., 2005. 2-Hydroxypropyl-β-cyclodextrin (HPβCD): A toxicology review. Food Chem. Toxicol. 43, 1451-1459.

Gupta, M., Sharma, R., Kumar, A., 2018. Docking techniques in pharmacology: How much promising? Comput. Biol. Chem. 76: 210-217.

Hendy, G.M., Breslin, C.B., 2011. A spectrophotometric and NMR study on the formation of an inclusion complex between dopamine and a sulfonated cyclodextrin host. J. Electroanal. Chem. 661, 179-185.

Hu, L., Xia, Z., 2018. Application of ozone micro-nano-bubbles to groundwater remediation. J. Hazard. Mater. 342, 446-453.

Karoyo, A.H., Wilson, L.D., 2019. A spectroscopic study of a cyclodextrin-based polymer and the “molecular accordion” effect. Can. J. Chem. 97, 442-450.

Khan, N.A., Carroll, K.C., 2020. Natural attenuation method for contaminant remediation reagent delivery assessment for in situ chemical oxidation using aqueous ozone. Chemosphere 247, 125848.

Khan, N.A., Johnson, M.D., Carroll, K.C., 2018. Spectroscopic methods for aqueous cyclodextrin inclusion complex binding measurement for 1, 4-dioxane, chlorinated co-contaminants, and ozone. J. Contam. Hydrol. 210, 31-41.

Khan, N.A., Johnson, M.D., Kubicki, J.D., Holguim, F.O., Dungan, B., Carroll, K.C., 2019. Cyclodextrin-enhanced 1,4-dioxane treatment kinetics with TCE and 1,1,1-TCA using aqueous ozone. Chemosphere 219, 335-344.

Kim, A.S., Cha, D., Lee, K., Lee, H., Kim, T., Lee, C., 2020. Modeling of ozone decomposition, oxidant exposures, and the abatement of micropollutants during ozonation processes. Water Res. 169, 115230.

Kim, A.S., Cha, D., Lee, K., Lee, H., Kim, T., Lee, C., 2020. Modeling of ozone decomposition, oxidant exposures, and the abatement of micropollutants during ozonation processes. Water Res. 169, 115230.

Lin, Z.Y., Liu, Y.X., Kou, S.B., Wang, B.L., Shi, J.H., 2020. Characterization of the inclusion interaction of ethinyloestradiol with β-cyclodextrin and hydroxypropyl-β-cyclodextrin: Multi-spectroscopic and molecular modeling methods. J. Mol. Liq. 311, 113290.

Liu, Q., Zhou, Y., Lu, J., Zhou, Y., 2020. Novel cyclodextrin-based adsorbents for removing pollutants from wastewater: A critical review. Chemosphere 241, 125043.

Lv, T., Zhang, Y., Zhang, L., Carvalho, P.N., Arias, C.A., Brix, H., 2016. Removal of the pesticides imazalil and tebuconazole in saturated constructed wetland mesocosms. Water Res. 91, 126-136.

Lyu, T., Zhang, L., Xu, X., Arias, C.A., Brix, H., Carvalho, P.N., 2018. Removal of the pesticide tebuconazole in constructed wetlands: Design comparison, influencing factors and modelling. Environ Pollut. 233, 71-80.

Manhas, M.S., Mohammed, F., Khan, Z., 2007. A kinetic study of oxidation of β-cyclodextrin by permanganate in aqueous media. Colloids Surf. A Physicochem. Eng. Asp. 295, 165-171.

Morris, G.M., Huey, R., Lindstrom, W., Sanner, M.F., Belew, R.K., Goodsell, D.S., Olson, A.J., 2009. AutoDock4 and AutoDockTools4: automated docking with selective receptor flexibility. J. Comput. Chem. 30, 2785-2791.

Nawrocki, J., Kasprzyk-Hordern, B., 2010. The efficiency and mechanisms of catalytic ozonation. Appl. Catal. B Environ. 99, 27-42.

Parmar, R., Majumder, S.K., 2015. Terminal rise velocity, size distribution and stability of microbubble suspension. Asia-Pac. J. Chem. Eng. 10, 450-465.

Prasse, C., Wagner, M., Schulz, R., Ternes, T.A., 2012. Oxidation of the antiviral drug acyclovir and its biodegradation product carboxy-acyclovir with ozone: kinetics and identification of oxidation products. Environ. Sci. Technol. 46(4), 2169-2178.

Rasdi, F.L.M., Rahim, N.Y., Hasim, F.W., Prabu, S., Jumbri, K., Manan, N.S.A., Mohamad, S., 2019. Influence of degree of substitution on the host-guest inclusion complex between ionic liquid substituted β-cyclodextrins with 2,4- dichlorophenol: An electrochemical, NMR andmolecular docking studies. J. Mol. Liq. 292, 111334.

Schneider C. A., Rasband, W. S., Eliceiri, K. W., 2012. NIH Image to ImageJ: 25 years of image analysis. Nat. methods. 9, 671-675, PMID 22930834

Shi, J.H., Zhou, Y.F., 2011. Inclusion interaction of chloramphenicol and heptakis (2,6-di-O-methyl)-β-cyclodextrin: Phase solubility and spectroscopic methods. Spectrochim. Acta A Mol. Biomol. Spectrosc. 83, 570-574.

Srinivasan, K., Stalin, T., Sivakumar, K., 2012. Spectral and electrochemical study of host-guest inclusion complex

between 2,4-dinitrophenol and β-cyclodextrin. Spectrochim. Acta A Mol. Biomol. Spectrosc. 94, 89-100.

Szente, L., Singhal, A., Domokos, A., Song, B., 2018. Cyclodextrins: Assessing the impact of cavity size, occupancy, and substitutions on cytotoxicity and cholesterol homeostasis. Molecules 23, 1228.

Van Aken, P., Lambert, N., Van den Broeck, R., Degrève, J., Dewil, R., 2019. Advances in ozonation and biodegradation processes to enhance chlorophenol abatement in multisubstrate wastewaters: a review. Environmental Science: Water Research & Technology. 5, 444-481.

Wang, J., Quan, X., Chen, S., Yu, H., Liu, G., 2019. Enhanced catalytic ozonation by highly dispersed CeO2 on carbon nanotubes for mineralization of organic pollutants. J. Hazard. Mater. 368, 621-629.

Wang, L., Ali, J., Wang, Z., Oladoja, N.A., Cheng, R., Zhang, C., Mailhot, G., Pan, G., 2020. Oxygen nanobubbles enhanced photodegradation of oxytetracycline under visible light: Synergistic effect and mechanism. Chemical Engineering Journal. 388, 124227.

Yang, J., Luo, C., Li, T., Cao, J., Dong, W., Li, J., Ma, J., 2020. Superfast degradation of refractory organic contaminants by ozone activated with thiosulfate: Efficiency and mechanisms. Water Res. 176, 115751.

Mehrjouei, M., Müller, S., Möller, D., 2015. A review on photocatalytic ozonation used for the treatment of water and wastewater. Chem. Eng. J. 263, 209-219.

Yuan, Y., Xing, G., Garg, S., Ma, J., Kong, X., Dai, P., Waite, D., 2020. Mechanistic insights into the catalytic ozonation process using iron oxide-impregnated activated carbon. Water Res. 177, 115785.

Zhang, C.L., Liu, J.C., Yang, W.B., Chen, D.L., Jiao, Z.G., 2017. Experimental and molecular docking investigations on the inclusion mechanism of the complex of phloridzin and hydroxypropylb- cyclodextrin. Food Chem. 215, 124-128.

Zhang, L., Lyu, T., Ramirez Vargas, C.A., Arias, C.A., Carvalho, P.N., Brix, H., 2018. New insights into the effects of support matrix on the removal of organic micro-pollutants and the microbial community in constructed

wetlands. Environ. Pollut. 240, 699-708.

Zhang, X. H.; Maeda, N.; Craig, V. S. J., 2006. Physical Properties of Nanobubbles on Hydrophobic Surfaces in Water and Aqueous Solutions. Langmuir 22, 5025-5035.

Zhou, Y., Hu, Y., Huang, W., Cheng, G., Cui, C., Lu, J., 2018. A novel amphoteric β-cyclodextrin-based adsorbent for simultaneous removal of cationic/anionic dyes and bisphenol A. Chem. Eng. J. 341, 47-57.

Zhou, Y., Liu, Q., Lu, J., He, J., Liu, Y., Zhou, Y., 2020. Accelerated photoelectron transmission by carboxymethyl β-cyclodextrin for organic contaminants removal: An alternative to noble metal catalyst. J. Hazard.Mater. 393, 122414.

Zimmerman, W.B., Tesař, V., Hemaka Bandulasena, H.C., 2011. Towards energy efficient nanobubble generation with fluidic oscillation. Curr Opin Colloid In 16, 350-6.